Hindawi Publishing Corporation
International Journal of Electrochemistry
Volume 2016, Article ID 4682967, 10 pages
http://dx.doi.org/10.1155/2016/4682967

Research Article

Nanoscaled Electrocatalytic Optically Modulated ZnO Nanoparticles through Green Process of *Punica granatum* L. and Their Antibacterial Activities

Xolile Fuku,[1,2] Abdoulaye Diallo,[1,2] and Malik Maaza[1,2]

[1] *UNESCO-UNISA Africa Chair in Nanosciences/Nanotechnology, College of Science, Engineering and Technology, University of South Africa, Muckleneuk Ridge, P.O. Box 392, Pretoria 0003, South Africa*
[2] *Nanosciences African Network (NANOAFNET), Materials Research Department, iThemba LABS-National Research Foundation of South Africa, Old Faure Road, P.O. Box 722, Somerset West, Western Cape 7129, South Africa*

Correspondence should be addressed to Xolile Fuku; xgfuku@gmail.com

Received 22 January 2016; Accepted 11 July 2016

Academic Editor: Shen-Ming Chen

Most recently, green synthesis of metal oxide nanoparticles has become an interesting subject of the nanoscience and nanotechnology. The use of plant systems has been deemed a green route and a dependable method for nanoparticle biosynthesis, owing to its environmental friendly nature. The present work demonstrates the bioreductive green synthesis of nanosized zinc oxide (ZnO) using peel extracts of pomegranate. Highly crystalline ZnO nanoparticles (ZnO NPs) which are 5 nm in particle size were characterised by HRTEM and XRD. FT-IR spectra confirmed the presence of the biomolecules and formation of plant protein-coated ZnO NPs and also the pure ZnO NPs. Electrochemical investigation revealed the redox properties and the conductivity of the as-prepared ZnO nanoparticles. The optical band gap of ZnO NPs was calculated to be 3.48 eV which indicates that ZnO NPs can be used in metal oxide semiconductor-based devices. Further, the nanomaterials were also found to be good inhibitors of bacterial strains at both low and high concentrations of 5–10 mg mL^{-1}.

1. Introduction

In recent years, nanotechnology has emerged as a state-of-the-art and cutting edge technology with various applications in a wide range of research fields. It is a very broad area comprising of cluster of nanomaterials, nanotools, and nanodevices. Most researchers have placed their focus mainly on nanoparticles synthesis as they can be easily prepared and manipulated [1–3]. Conventional methods of synthesis such as physical and chemical methods have been employed in the synthesis of these nanomaterials. However, these methods have several limitations due to toxicity, being time consuming, and requiring high temperature conversion [4, 5]. In view of simplicity, low cost involvement, higher reducing potential, and less environmental impact, research focus has shifted towards the development of clean and eco-friendly synthesis protocols [4, 6, 7]. The green method of synthesis is easy, efficient, and eco-friendly relative to chemically mediated synthesis [4, 8, 9]. A wide variety of biological resources like microorganisms (bacteria, yeast, fungi, algae, and viruses) and plants [4, 10] have recently gained attention for the synthesis of metal and metal oxide nanoparticles. Amid these, biosynthesis of nanoparticles (NPs) from plants seems to be an efficient method in developing clean, nontoxic, and eco-friendly technologies. Different plant groups from algae to angiosperms possess different phytochemicals which act as protective agent against UV light, heavy metal toxicity, and reducing agents [11, 12]. For this reason, several metal oxides NPs have and still are being synthesised using green processes. Ahmad et al. studied rapid green synthesis of silver and gold nanoparticles using peels of *Punica granatum* [12] while Das et al. reported a one-step green synthesis and characterisation of plant protein-coated mercuric oxide (HgO) nanoparticles: antimicrobial studies [13] and Ramesh and Meenakshisundaram synthesised zinc oxide NPs using flower extract of *Cassia auriculata* [14]. ZnO is one of the

main metal oxides which have been studied extensively using both chemical and green processes [1, 15]. ZnO NPs are known to be multifunctional semiconducting materials [15–17] with a wide band gap and large exciton binding energy [18–21]. Additionally, ZnO exhibits several promising prospects for nanoscale structures. One-dimensional (1D) ZnO semiconductor has been investigated in a wide range of applications, such as room temperature ultraviolet (UV) lasers, surface-acoustic-wave devices, gas sensors, solar cells, infrared sensors, optoelectronic devices, and electronic paper [17, 22–24]. Combining the proper energy level and high electronic mobility, ZnO could create a suitable material for the photoanode in dye-sensitized solar cells and ultracapacitors [15, 22, 24–26]. Further, nanosized ZnO NPs illustrate significant antibacterial activity over a wide spectrum of bacterial species explored by various researchers [27–29]. Since the nanooxides have been studied at both micro- and nanometer range, it has been established that ZnO NPs exhibit significant antimicrobial activities when particle size is reduced to the nanometer range. The nanooxides can interact with bacterial surface and/or with the bacterial core when entering the cell and consequently exhibit individual bactericidal mechanisms [28, 30]. In this view, we present a simple and new eco-friendly biosynthesis of ZnO nanoparticles using pomegranate peel extract as the reducing agent. In this paper, the nanooxides will be synthesised in view of studying them in different applications and/or fields. Chemical constituents of pomegranate peel extract will be used in the synthesis of ZnO NPs as both reducing and stabilizing ligands. The as-prepared nanoparticles will be characterised using optical, microscopic, and electrochemical methods, that is, UV-vis, Fourier transform infrared spectroscopy (FTIR), photoluminescence (PL), high resolution transmission electron microscopy (HRTEM), high resolution scanning electron microscopy (HRSEM), X-ray diffraction (XRD), electrochemical impedance (EIS), and cyclic voltammetry (CV).

2. Experimental Procedures

2.1. Reagents and Materials. Zinc nitrate salt ($Zn(NO_3)_2 \cdot 6H_2O$ 99.98%) and silver/silver chloride (Ag/AgCl, 3 M), polystyrene graduated tubes, and 0.22 μm hydrophilic filters (Whatman) were purchased from Sigma-Aldrich. Phosphate buffer solution (PBs), 0.1 M, pH 7.0 was prepared from anhydrous potassium hydrogen phosphate (K_2HPO_4) and potassium dihydrogen phosphate (KH_2PO_4). Gram-negative and Gram-positive bacterial species *(E. coli-K12, P. vulgaris-ATCC-49132,* and *S. aureus-MRSA-33591)* and both antibiotics *(Streptomycin and Gentamicin)* were purchased from Sigma-Aldrich. Purified deionized water was used for aqueous solution preparations. All chemicals were supplied by Sigma-Aldrich and Metrohm.

2.1.1. One-pot Synthesis of ZnO Nanoparticles. 40 g peels of pomegranate were added into a 250 mL round bottle of deionised water (40°C), and a yellow to reddish brown extract was formed at pH 3. The broth/extract was filtered with Whatman paper (0.22 μm). 8 g of the zinc nitrate salt was then dissolved in 200 mL of pomegranate broth (80°C), after which a yellow precipitate of ZnO nanoparticles (pH 5) was formed (Scheme 1).

For X-ray diffraction (XRD) analysis, the precipitate was collected via centrifugation (10 min, 1000 rpm) and the materials were washed with distilled water several times in order to remove free ions, using a combination of sonication and centrifugation. 70% yield of the powdered nanoparticles (ZnO) was realised and was dried in an oven at 100°C, 15 min. The as-prepared ZnO nanoparticles were then crashed into a powder using mortar and pestle, after which the nanomaterials were annealed at different temperature (400°C and 500°C). The ZnO nanoparticles were redispersed in 0.1 M phosphate buffer (pH 7.4) for further spectroscopic, microscopic, and electrochemical analyses.

2.1.2. Preparation of ITO/ZnO Electrodes. Indium tin oxide (ITO) electrode was thoroughly cleaned by sonication in absolute ethanol and deionized water (5 min), respectively, and finally rinsed with distilled water. The electrode (ITO) was drop-coated with ZnO NPs solution (60 μL), dried at 50°C for 15 min, and gently washed with deionised water to remove any loosely bound material. The electrode was labelled as ITO/ZnO. Phosphate buffer solution (0.1 M, pH 7) was used as electrolyte for electrochemical measurements.

2.1.3. Antibacterial Activity. Antibacterial activity was screened against three bacterial strains, namely, Gram-negative and Gram-positive bacteria *S. aureus, P. vulgaris*, and *E. coli*. Six plates were prepared and swabbed using sterile long-shaped rod with 1 mL of mature (24 h) broth culture of individual bacterial strains. The wells were made by using sterile cork borer (600 mm) which were created into Petri-dishes. Varied concentrations of ZnO NPs (10 mg mL^{-1} and 5 mg mL^{-1}) were used to measure the activity of the nanooxides. By well diffusion method, 6 mm discs were used for diffusion of NPs broth. Simultaneously the standard antibiotics as positive and negative controls were tested against the bacterial pathogens. Then the plates were incubated at 37°C for 24 h; the zone inhibition was measured in millimeter (mm) for every well.

2.2. Instrumentation and Electrochemical Measurements

2.2.1. Instrumentation. The surface morphology, size, and distribution of the synthesised ZnO nanoparticles were examined using transmission electron microscope (TEM, JEOL 2011). TEM was operated at 200 kV using a LaB6 filament equipped with a Gatan multiscan camera 794 and the sample was dropcast onto Cu grids. Elemental analysis was enabled using EDX/EDS and X-ray diffraction (XRD) performed using a Rigaku D/MAX-PC 2500 X-ray diffractometer with a CuK_α ($\lambda = 1.54$ Å) radiation source operating at 40 kV and 200 mA. Fourier transform infrared spectroscopy (FTIR) experiments were performed on a Perkin Elmer spectrometer (Spectrum 100), fluorescence experiments were performed on Type FL3-2IHR, and UV-vis absorption spectroscopy was performed using Nicolet Evolution 100, Thermo Electron. Electrochemical experiments {cyclic voltammetry

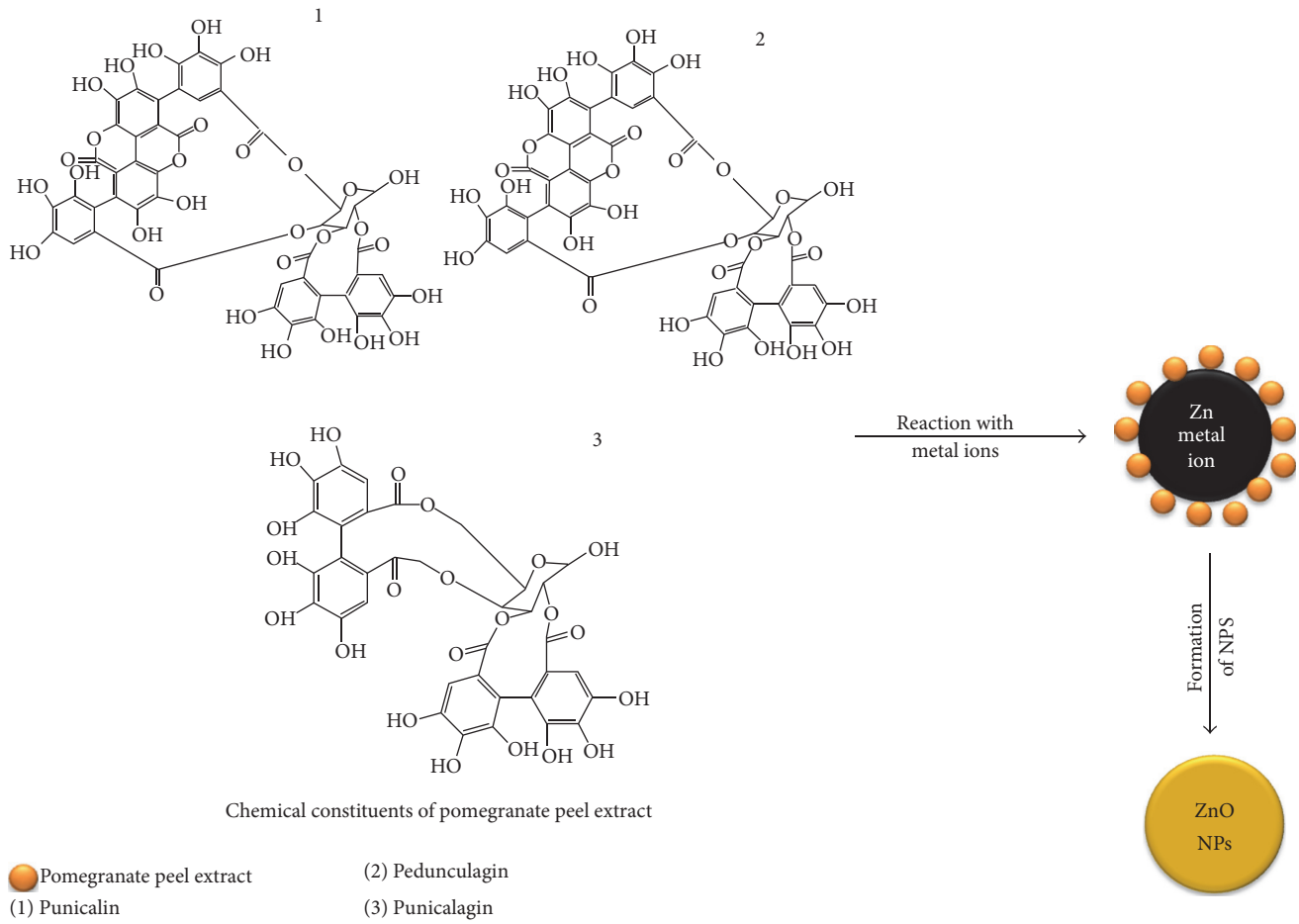

Scheme 1: Schematic representation of ZnO nanoparticle synthesis.

(CV) and electrochemical impedance spectroscopy (EIS)} were performed using Autolab Instruments, Metrohm. A three-electrode electrochemical cell comprising a platinum counter electrode, Ag/AgCl reference electrode, indium tin oxide glass (ITO) working electrode, and 0.1 M PBS (pH 7) as electrolyte was used in all electrochemical experiments.

3. Results and Discussion

3.1. Formation and Structural Characterisation of ZnO Nanoparticles. The particle size and surface morphology of the resultant ZnO nanoparticles (ZnO NPs) were characterised with the help of HR-TEM and HRSEM (Figures 1(a)–1(f) and Figures 2(a)-2(b)), respectively. The used techniques provided evidence of particle distribution, indicating that the synthetic route was successful. Figures 1(a) and 1(b) show ZnO NPs before and after annealing. Compared to the unannealed ZnO NPs, the annealed ZnO NPs revealed smaller particle size with slight agglomeration. From HRTEM images, the average diameter ($n = 10$) of the NPs was estimated to be 20 ± 5 nm. Diffraction patterns observed from Figures 1(c) and 1(d) confirmed crystallinity of the annealed NPs relative to the unannealed nanomaterials. HRTEM images showed the unidirectional lattice fringes (d spacing = 0.1 nm), confirming the monocrystallinity of the annealed material (Figures 1(e) and 1(f)). It is evident that the as-prepared ZnO NPs required heating in order to reveal or elucidate their cubic and/or crystalline nature.

HR-SEM and EDS were employed to further investigate the structural morphology and the constituents of the as-synthesised ZnO NPs. HR-SEM data confirmed that the structural nature of ZnO NPs is cubic. The good correlation between particle sizes obtained from HR-SEM and HR-TEM supports the morphological structure of the Zinc NPs and is also reviewed in literature [14, 31]. EDX spectrum indicates that the as-prepared products of green process are composed of zinc (Zn) and oxygen (O) of 68.30 and 31.70% (Figure 2(b)). Au and Pd elements are due to substrate modification.

The structural and size verification of the ZnO NPs were further investigated by using XRD. Figure 3((A), (B), and (C)) shows diffraction patterns of ZnO NPs at different temperatures, that is, ambient temperature, 400°C and 500°C. Compared to ZnO NPs at 400°C (Figure 3(B)), nanoparticles at 500°C showed clear distinctive diffraction peaks (Figure 3(C)), while unannealed nanomaterials (Figure 3(A)) showed no diffraction peaks, indicating that the NPs are not highly crystalline at this temperature. XRD analysis

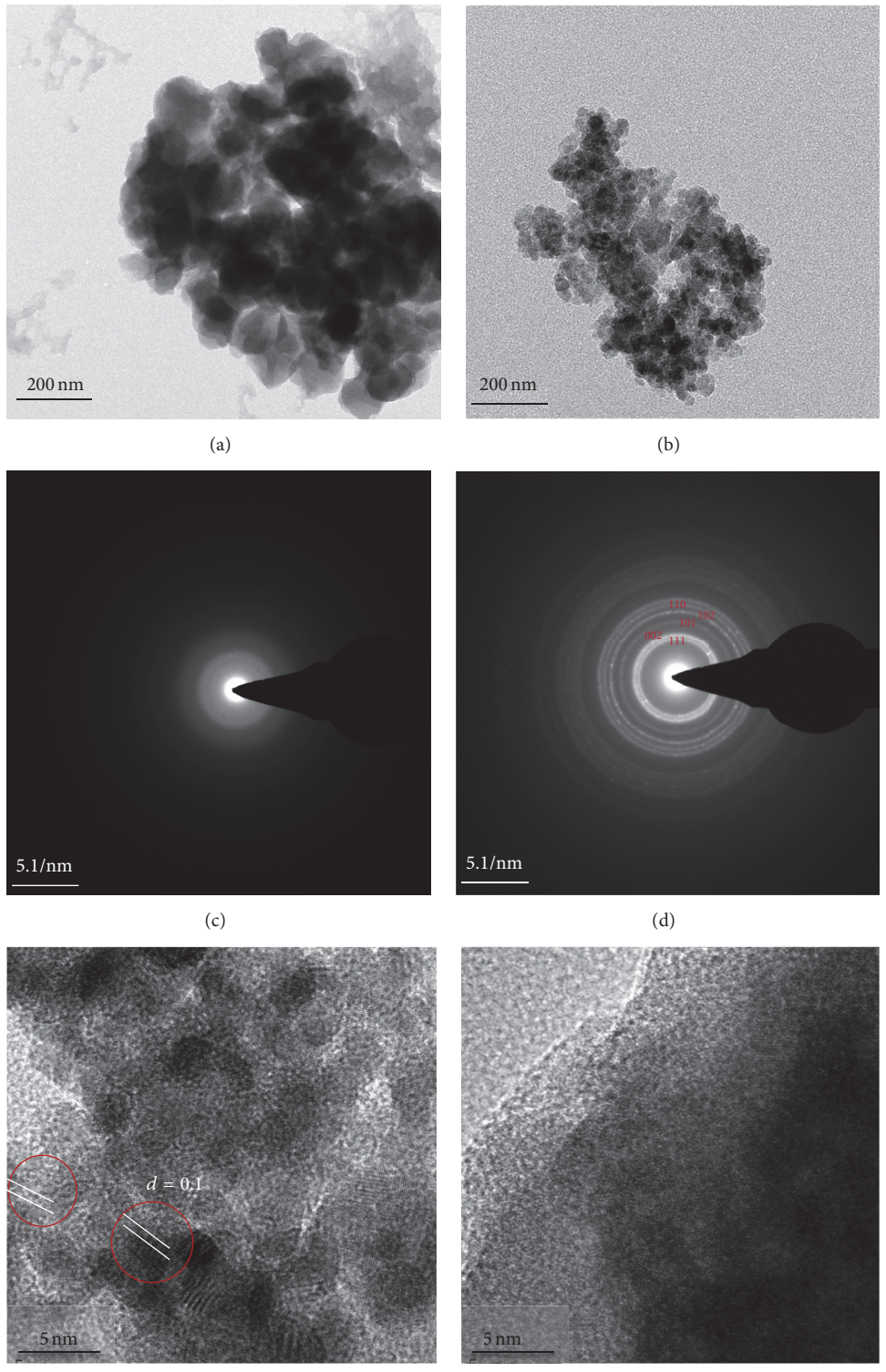

Figure 1: HRTEM analysis for ZnO nanoparticles sample (a–f) TEM images.

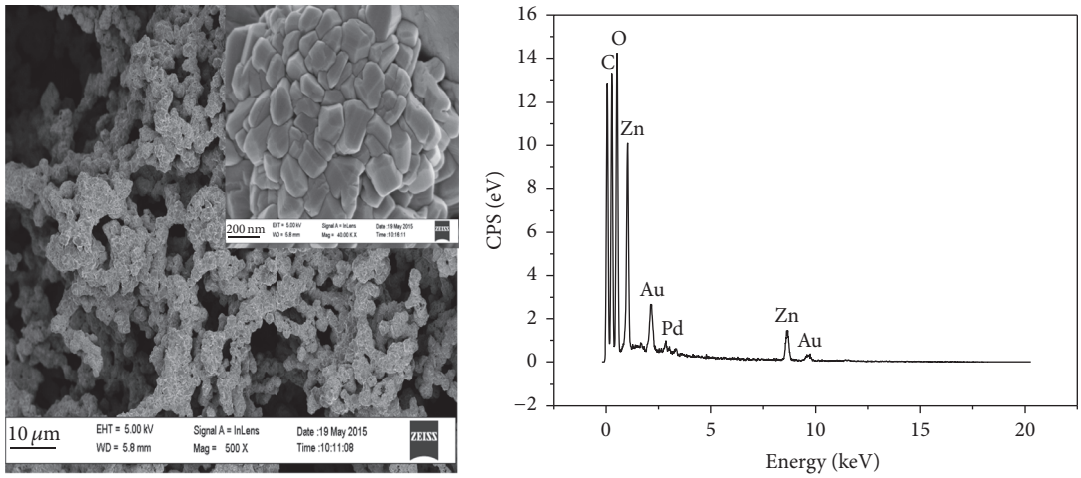

Figure 2: HRSEM analysis for ZnO nanoparticles sample (a) SEM images and (b) EDS spectrum for ZnO.

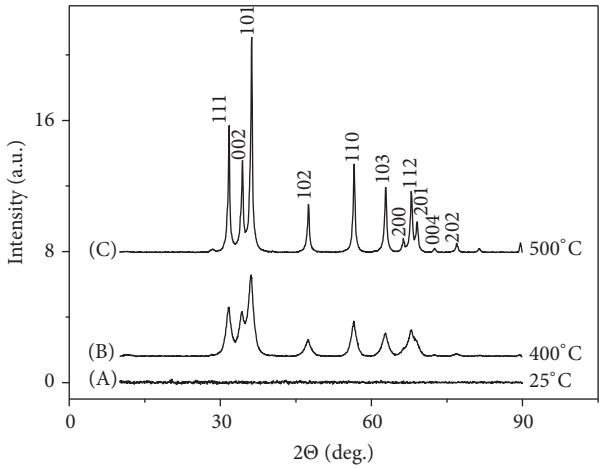

Figure 3: XRD spectra of ZnO nanoparticles (A) before annealing and (B, C) after annealing.

(Figure 3(C)) shows the diffraction pattern with peaks positions corresponding to crystal planes (111), (002), (101), (102), (110), (103), (200), (112), and (201) [14, 31–34]. The peaks of the graph are in good agreement with literature reports [16, 31, 33, 35].

From careful analysis of the peak positions and in accordance with the literature [33, 36], XRD patterns of the nanoparticles were indexed to the hexagonal wurtzite phase structure of ZnO [33] with lattice constants $a = b = 0.324$ nm and $c = 0.521$ nm. The acquired spectra confirmed that the synthesised nanopowder was free of impurities, evident by characteristic peaks of ZnO NPs only. In the XRD patterns, the (101) plane corresponding to 36.8° was found to be very clear and abundant which indicates preferential growth of the crystallites. The average size was calculated using the Scherrer equation [16, 32, 34, 37]:

$$d = \frac{0.9\lambda}{\beta \cos\theta}, \quad (1)$$

where d is the crystallite size, λ is the wavelength of X-ray used (1.5418 Å), β is the full width at half maximum, and θ is Bragg's angle of reflection. The average particle size calculated from (1) was 7 nm, which is in accord with the average size obtained from the HRTEM analysis.

FTIR spectroscopy was employed to confirm the formation, nonagglomeration, stability, reduction, and purity and also to identify the functional groups of the active components in the synthesised ZnO NPs. Figure 4 shows FTIR spectra of (a) pomegranate extract, (b) ZnO nanopowder before annealing, and (c) ZnO-NPs after annealing (500°C), synthesised in pomegranate peel broth. Pomegranate peel broth acted as capping and reducing agent preventing the aggregation of nanoparticles in solution and thus playing a relevant role in their extracellular synthesis and shaping. Figure 4(a) contains the FTIR spectrum of pomegranate peel broth which has vibrational stretches at 3500, 2200, and 1600 cm^{-1} due to OH, COO-, and C=O, respectively. Compared to the control (pomegranate peel broth alone, Figure 4(a)), the intensity of all vibrational stretches in the as-prepared NPs samples (Figures 4(b) and 4(c)) decreased with a slight shift in wavenumbers, indicating that the ZnO NPs were sufficiently capped and reduced with pomegranate peel extract. Relative to the unannealed NPs (Figure 4(b)), the annealed ZnO (Figure 4(c)) NPs showed a decrease and a disappearance of -OH, COO-, and C=O vibrational stretches. However, the C-O and ZnO stretches were observed at 500 cm^{-1} and 1.021 cm^{-1}, respectively. The formation of ZnO is characterised by an absorption band at 500 and 307 cm^{-1} which correspond to the Zn-O bond.

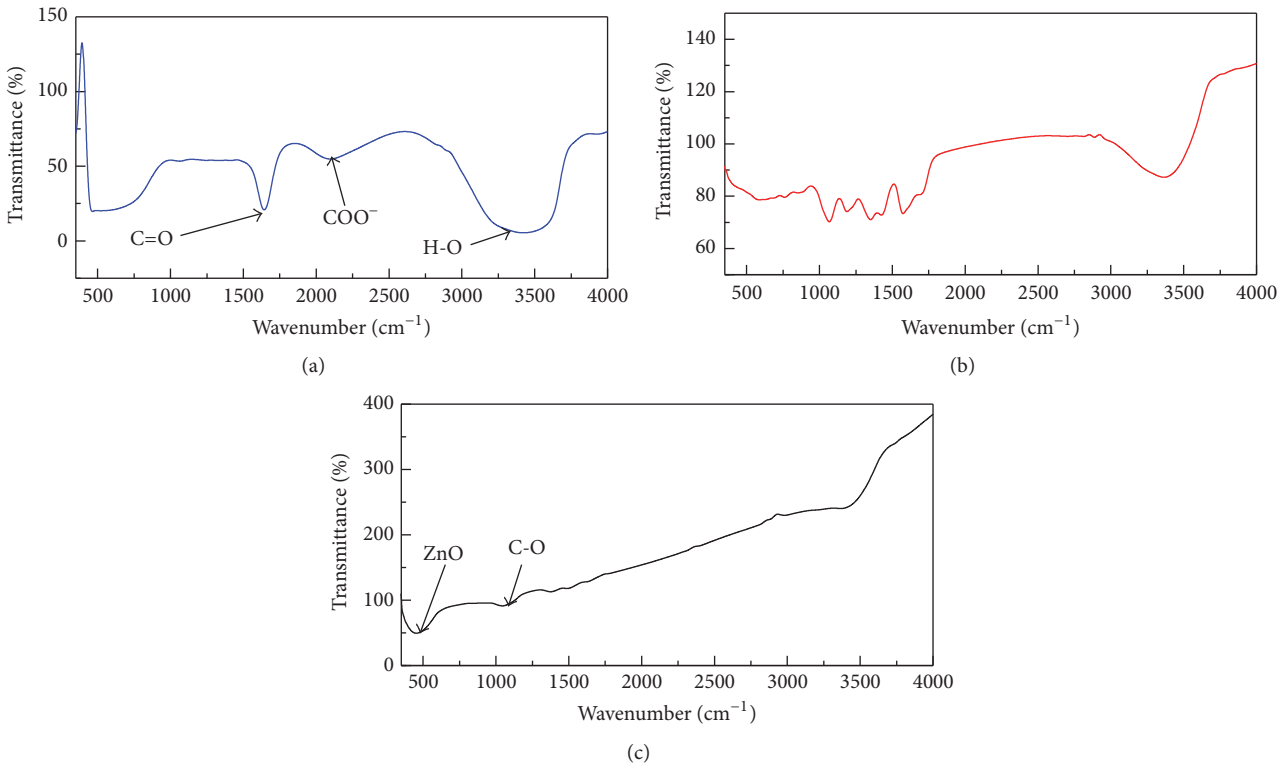

Figure 4: FTIR spectra of (a) pomegranate broth, (b) ZnO before annealing, and (c) ZnO after annealing.

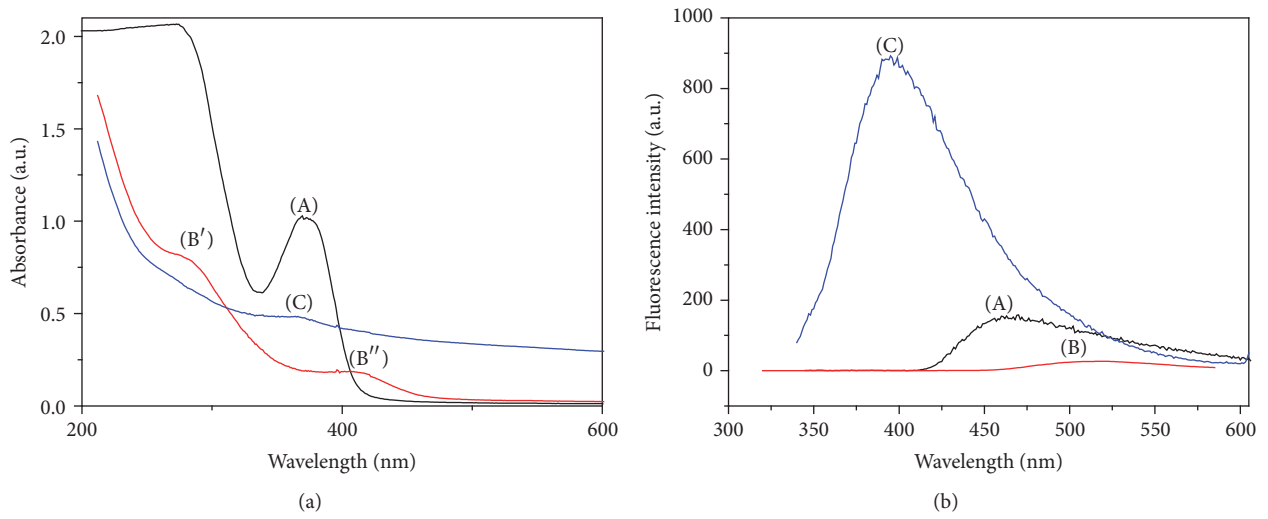

Figure 5: UV-vis spectra (a) and fluorescence spectra (b) of ZnO nanoparticles before and after annealing.

Figure 5 shows the UV-vis and fluorescence spectra of the pomegranate extract, as-prepared ZnO nanoparticles before and after annealing in solution. From UV-vis spectra, two clear distinctive absorption peaks of pomegranate were observed at 375 nm (Figure 5(a)(A)). However, a shift and a decrease in λ_{max} of ZnO nanoparticles before annealing was observed at 280 nm (Figure 5(a)(B′)) and at 412 nm (Figure 5(a)(B″)), confirming the formation of the as-synthesised nanomaterials. Moreover, the two absorption peaks merged into one resultant peak (Figure 5(a)(C), 366 nm) which was denoted to the pure ZnO NPs after annealing. λ_{max} of pure ZnO nanoparticles show good blue shift in wavelength.

Figure 5(b) depicts the fluorescence spectra of pomegranate extract, nanosized ZnO NPs before and after annealing. Strong emission peak centred at 395 nm was observed in pomegranate extract (Figure 5(b)(C)). The as-synthesised ZnO sample (before annealing) exhibits emission peaks

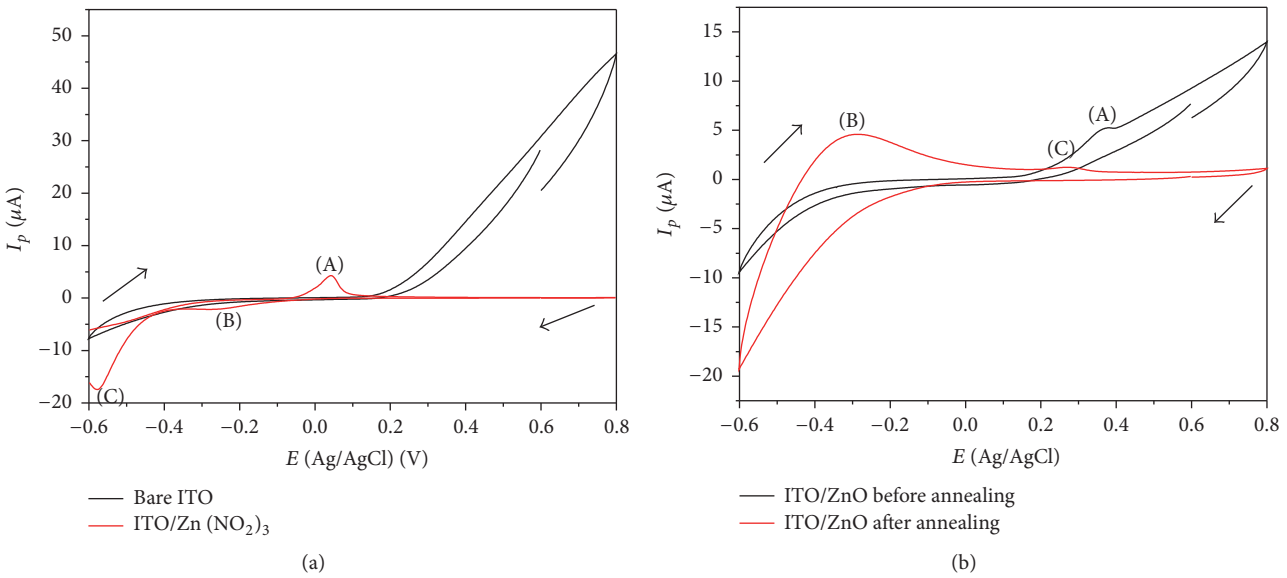

FIGURE 6: Cyclic voltammetric responses of electrode systems. (a) CVs of bare ITO and (b) ITO/ZnO before and after annealing. Experiments were carried out in 0.1 M PBS (pH = 7) at 50 mV s^{-1}.

at 462 nm and at 509 nm (after annealing). These results confirm the formation of ZnO NPs, apparent by a shift in wavelength (blue shift) from 395 to 462 nm. The emission peak at 462 nm corresponds to the near band gap excitonic emission and that at 509 is attributed to the pure ZnO NPs suggesting that our synthetic route is of high quality due to low concentration of singly ionized oxygen emission defects (at 530 nm), as reviewed from literature [38–41]. The emission is known to be caused by the radiative recombination of a photogenerated hole with an electron occupying the oxygen vacancy [28, 40]. From the 509 nm emission peak the band gap energy of the nanosized ZnO was calculated using Planck's equation and was found to be 3.4 eV, which is comparable with that observed in UV-vis and literature [35, 37–39, 41]. Consider

$$E_g = \frac{hc}{\lambda}, \tag{2}$$

where E_g is the band gap energy, h is the Planck constant (6.626×10^{-34} J s or 4.136×10^{-15} eV s), c is the speed of light = 3.0×10^8 m s^{-1}, and λ is the wavelength (509 and 366 × 10^{-9} m).

3.2. Electrochemical Characterisation of ZnO Nanoparticles. Cyclic voltammetry was employed to investigate the redox properties of ZnO NPs immobilised on indium tin oxide (ITO) electrode. Figure 6(a) shows the CVs of the bare ITO and ITO/$Zn(NO_2)_3$ in solution. Compared to bare electrode in aqueous medium (phosphate buffer solution), ITO electrode with zinc nitrate possesses two anodic peak currents ($I_{p,a}$) at $E_{p,a}$ = −0.25 V; −0.58 V (Figure 6(a)(B) and (C)) and cathodic peak currents ($I_{p,c}$) at $E_{p,c}$ = 0.14 V (Figure 6(a)(A)). The observed peak potentials are also obtained by other researchers [18, 31].

Figure 6(b) shows cyclic voltammograms of ITO/ZnO before and after annealing. The ZnO NPs (before annealing) exhibited its individual characteristic oxidation peak current at $E_{p,a}$ = 0.36 V (Figure 6(b)(A)) which shifted and gave two oxidation peaks at $E_{p,a}$ = 0.26 V and $E_{p,c}$ = −0.29 V (Figure 6(b)(B) and (C)), after annealing of the nanomaterials at 500°C. In accordance with literature [42, 43], the peak current at −0.29 V corresponds to the reduction of zincate, which can be due to controlled nucleation of ZnO NPs. Thus, from the results one can deduce that green synthesised ZnO NPs are redox active.

To further investigate the electron transfer kinetics at the electrode interface (ITO/ZnO), we applied electrochemical impedance spectroscopy (Figure 7). Figure 7(a) shows Nyquist plots of ITO/bare, ITO/zincate, and ITO/ZnO and the corresponding bode plots (Figure 7(b)). Parameters such as electron charge transfer resistance (R_{ct}) and the capacitance (CPE) were obtained by simulating the curves using the Randle Sevcik circuit (Figure 7(a): an insert). The Nyquist plot of the ZnO NPs depicts well-defined frequency-dependent semicircle impedance of curves over high frequencies. Furthermore, the ZnO NPs show smaller mass transfer (R_{ct}: 10.2 Ω) relative to that of both bare/ITO = 20.6 Ω and ITO/zincate = 14.9 Ω. The obtained results indicate that the presence of ZnO NPs at the electrode interface plays a pivotal role in increasing the electron transfer kinetics between electrolyte-transducer interface. Additionally, it is apparent from the plots that the ZnO NPs possess a catalytic behaviour. The surface coverage (θ) of ITO/ZnO was 0.78 cm s^{-1} and the electron transfer rate constant (k_{et}) values for bare ITO = 2.79×10^{-11}, ITO/zincate = 2.48×10^{-10}, and ITO/ZnO = 3.22×10^{-10} (at 280 mV) were calculated as shown in Table 1, respectively.

The corresponding bode plot (Figure 7(b)) substantiates the electrical properties of the nanoparticles. The obtained

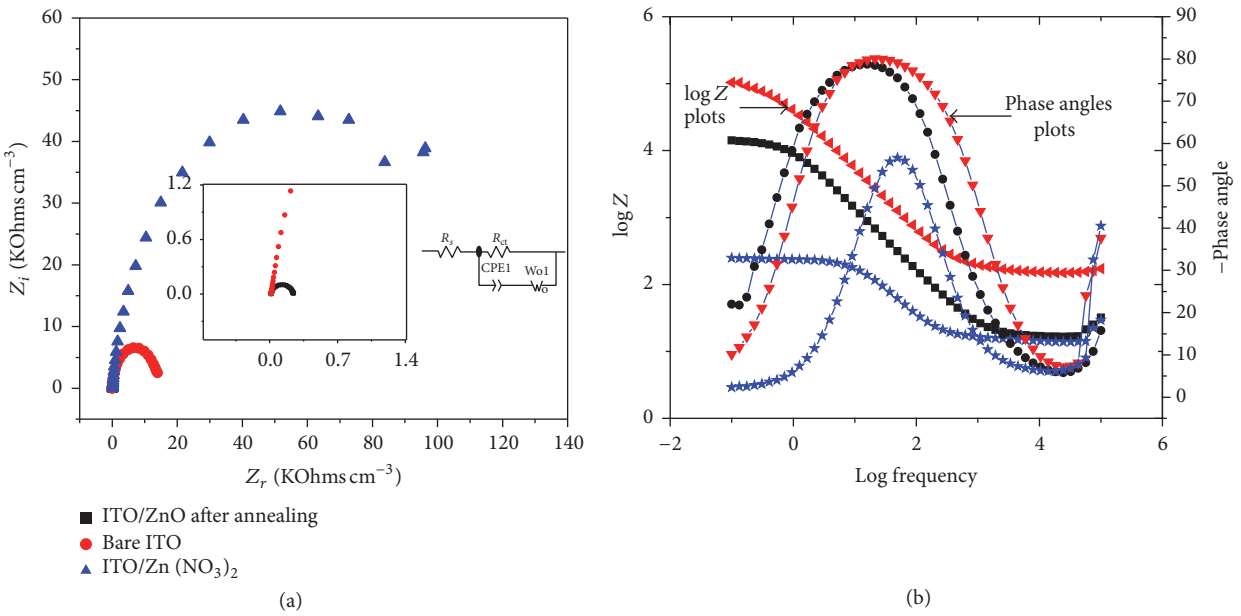

FIGURE 7: (a) Nyquist plots of bare ITO (blue symbols), ITO/zincate (red symbols), and ITO/ZnO (black symbols) electrodes in 0.1 M PBS (pH = 7.4). (b) The corresponding bode plots of the EIS data in (a).

TABLE 1: EIS parameters for ZnO nanoparticles.

Parameters	R_{ct} (Ω)	K_{et} (s^{-1})
ITO/bare	20.6	2.79×10^{-11}
ITO/zincate	14.9	2.48×10^{-10}
ITO/ZnO	8	3.22×10^{-10}

results are in union with the Nyquist plots, where the ITO/ZnO electrode showed improved conductivity based on the phase angle of the NPs. The actual phase angles for ITO/bare, ITO/zincate, and ITO/ZnO were found to be 55θ, 80θ, and 78θ, respectively. Relative to unmodified electrodes (ITO/Bare), the modified electrode (ITO/ZnO) is more conducting due to the contribution of solution resistance (R_s), charge transfer resistance (R_{ct}), and capacitance (CPE) in the electrical circuit, which are more predominant, meaning that the R_{ct} is more predominant than *Rs*. The total impedance, Z, data of Figure 5(b) confirmed the conductive nature of the ITO/ZnO. However, the ITO/zincate electrode shows high phase angle (80θ) which was expected since the electrode is coated with conducting material. At $\log F = 0$, $\log Z$ (ITO/ZnO) = 4.2, whereas $\log Z$ (bare Au) = 2.3 and $\log Z$ (ITO/zincate) = 5. This means that when the electrode systems were subjected to nominal frequency effects the NPs become more conducting. There is a shift log 2 magnitude shift (increase) in frequency on changing from ITO/zincate (1.8) electrode to ITO/ZnO (1.4) electrode.

3.3. Antimicrobial Activity. To ascertain the antibacterial activity of ZnO NPs the pathogenic bacteria, such as *Escherichia coli (E. coli), Staphylococcus aureus (S. aureus),* and *Proteus vulgaris (P. vulgaris)* strains, were chosen for

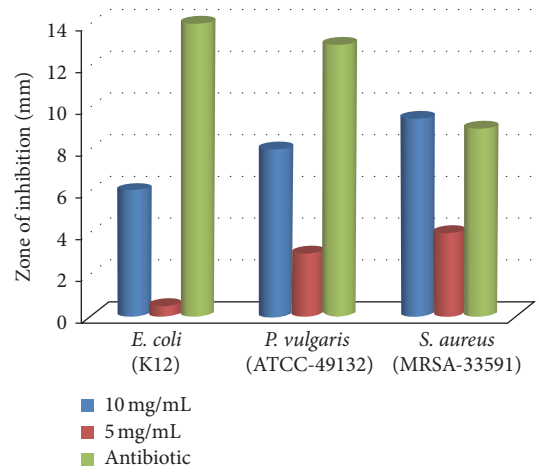

FIGURE 8: Representing zone of inhibition of ZnO nanoparticles tested on various bacterial species *(E. coli-K12, P. vulgaris-ATCC-49132,* and *S. aureus-MRSA-33591).*

the investigation. According to XRD and HRTEM, nanoparticle size of 7–200 nm was used (concentrations of 5 and 10 mg mL^{-1} (Table 2)) against different pathogenic bacteria, that is, *E. coli, S. aureus,* and *P. vulgaris*. Further, the antibacterial activity of the synthesised zinc oxide nanoparticles was compared to that of the two antibiotics *(Streptomycin and Gentamicin)* by using disc (6 mm) diffusion test. Figure 8 represents the antibacterial activity of ZnO NPs for various bacteria in a well diffusion assay.

The antibacterial analyses data (Figure 8) denotes that ZnO NPs (size of 7–200 nm) have shown potential activity against the tested bacteria at different concentrations. ZnO

Table 2: Antibacterial activity of CuO NPs on various bacterial species *(E. coli-K12, P. vulgaris-ATCC-49132,* and *S. aureus-MRSA-33591)*.

Conc (mg mL^{-1})	*E. coli (K12)*	*P. vulgaris (ATCC-49132)*	*S. aureus (MRSA-33591)*
5	0.5	3	4
10	6	8	9.5
Antibiotic	14	13	9
		Zone of inhibition (mm)	

NPs had more activity against *S. aureus* than both *E. coli* and *P. vulgaris*. Meanwhile, *S. aureus* and *P. vulgaris* were more susceptible to ZnO NPs than *E. coli*. Moreover, ZnO NPs showed increased zone of inhibition at higher concentrations (10 mg mL^{-1} ZnO NPs) than at lower concentration (5 mg mL^{-1} ZnO NPs) thus confirming the antibacterial activity of ZnO NPs at these concentrations. However, the antibiotics showed higher activity than the nanoparticles. The results obtained are in agreement with those reviewed in literature [28, 44, 45]. In summary, it is lucid that at high concentrations ZnO NPs retard the growth of all the pathogens when they are present in the bacterial suspension, thus confirming the dependence of ZnO NPs on concentration to inhibit the bacteria.

4. Conclusion

Hitherto, there is no report of synthesis of ZnO nanoparticles using peel extracts of *Punica granatum* L. Pure ZnO NPs were successfully synthesised and characterised using surface, structural, electrochemical, and spectroscopic techniques. Formation of ZnO NPs using green process was confirmed by FTIR studies, which showed characteristic bands related to ZnO and C-O groups. Optical and electrochemical methods were able to determine the conductivity of the NPs and semiconductor properties of the nanooxides. The green synthesis approach shows that the environmentally friendly peel extract of *Punica granatum* L. can be used as an efficient stabilizing, capping, and reducing agent for the synthesis of ZnO and other nanoparticles. Furthermore, ZnO NPs demonstrated excellent antimicrobial activity against a range of bacteria at two different concentrations. In this regard, these significant findings of ZnO NPs on various bacterial strains should enthuse one to study a whole range of bacterial species. Thus far, our findings hold a significant potential in a wide variety of applications such as energy, nanoelectronic, bio/sensing devices, photocatalytic, and microbial activities because of the green process pollution-free and eco-friendly approach. These findings should encourage possible core-shell structure of the ZnO nanocomposite in future work.

Competing Interests

The authors declare that they have no competing interests.

Acknowledgments

The authors acknowledge Postdoctoral Fellowship Bursary from UNESCO-UNISA Africa Chair in Nanosciences/Nanotechnology funding and iThemba LABS-National Research Foundation of South Africa (Material Science Department) for the use of their research labs and offices.

References

[1] G. Yang, F. Chen, and Z. Yang, "Electrocatalytic oxidation of hydrogen peroxide based on the shuttlelike nano-CuO-modified electrode," *International Journal of Electrochemistry*, vol. 2012, Article ID 194183, 6 pages, 2012.

[2] S. H. Yu and G. C. Zhao, "Preparation of platinum nanoparticles-graphene modified electrode and selective determination of rutin," *International Journal of Electrochemistry*, vol. 2012, Article ID 431253, 6 pages, 2012.

[3] S. C. Pang, B. H. Wee, and S. F. Chin, "The capacitive behaviors of manganese dioxide thin-film electrochemical capacitor prototypes," *International Journal of Electrochemistry*, vol. 2011, Article ID 397685, 10 pages, 2011.

[4] M. S. Akhtar, J. Panwar, and Y.-S. Yun, "Biogenic synthesis of metallic nanoparticles by plant extracts," *ACS Sustainable Chemistry and Engineering*, vol. 1, no. 6, pp. 591–602, 2013.

[5] M. Potara, M. Bawaskar, T. Simon et al., "Biosynthesized silver nanoparticles performing as biogenic SERS-nanotags for investigation of C26 colon carcinoma cells," *Colloids and Surfaces B: Biointerfaces*, vol. 133, pp. 296–303, 2015.

[6] A. K. Mittal, Y. Chisti, and U. C. Banerjee, "Synthesis of metallic nanoparticles using plant extracts," *Biotechnology Advances*, vol. 31, no. 2, pp. 346–356, 2013.

[7] N. L. Gavade, A. N. Kadam, M. B. Suwarnkar, V. P. Ghodake, and K. M. Garadkar, "Biogenic synthesis of multi-applicative silver nanoparticles by using *Ziziphus Jujuba* leaf extract," *Spectrochimica Acta Part A: Molecular and Biomolecular Spectroscopy*, vol. 136, pp. 953–960, 2015.

[8] R. Rajan, K. Chandran, S. L. Harper, S.-I. Yun, and P. T. Kalaichelvan, "Plant extract synthesized silver nanoparticles: an ongoing source of novel biocompatible materials," *Industrial Crops and Products*, vol. 70, pp. 356–373, 2015.

[9] S. S. Sana, V. R. Badineni, S. K. Arla, and V. K. N. Boya, "Eco-friendly synthesis of silver nanoparticles using leaf extract of *Grewia flaviscences* and study of their antimicrobial activity," *Materials Letters*, vol. 145, pp. 347–350, 2015.

[10] K. B. Narayanan and N. Sakthivel, "Biological synthesis of metal nanoparticles by microbes," *Advances in Colloid and Interface Science*, vol. 156, no. 1-2, pp. 1–13, 2010.

[11] M. Ganeshkumar, M. Sathishkumar, T. Ponrasu, M. G. Dinesh, and L. Suguna, "Spontaneous ultra fast synthesis of gold nanoparticles using *Punica granatum* for cancer targeted drug delivery," *Colloids and Surfaces B: Biointerfaces*, vol. 106, pp. 208–216, 2013.

[12] N. Ahmad, S. Sharma, and R. Rai, "Rapid green synthesis of silver and gold nanoparticles using peels of *Punica granatum*," *Advanced Materials Letters*, vol. 3, no. 5, pp. 376–380, 2012.

[13] A. K. Das, A. Marwal, D. Sain, and V. Pareek, "One-step green synthesis and characterization of plant protein-coated mercuric oxide (HgO) nanoparticles: antimicrobial studies," *International Nano Letters*, vol. 5, no. 3, pp. 125–132, 2015.

[14] P. Ramesh and M. Meenakshisundaram, "Green syntheis of zinc oxide nanoparticles using flower extract cassia auriculata," *Journal of Nanoscience and Nanotechnology*, vol. 2, no. 1, pp. 41–45, 2014.

[15] I. E. Paulauskas, G. E. Jellison Jr., L. A. Boatner, and G. M. Brown, "Photoelectrochemical stability and alteration products of n-type single-crystal ZnO photoanodes," *International Journal of Electrochemistry*, vol. 2011, Article ID 563427, 10 pages, 2011.

[16] R. Imani, V. Kononenko, T. Romih et al., "Growth of a novel nanostructured ZnO urchin: control of cytotoxicity and dissolution of the ZnO urchin," *Nanoscale Research Letters*, vol. 10, article 441, 2015.

[17] X. Qian, H. Liu, Y. Guo, Y. Song, and Y. Li, "Effect of aspect ratio on field emission properties of ZnO nanorod arrays," *Nanoscale Research Letters*, vol. 3, no. 8, pp. 303–307, 2008.

[18] F. Alvi, M. K. Ram, H. Gomez, R. K. Joshi, and A. Kumar, "Evaluating the chemio-physio properties of novel zinc oxide-polyaniline nanocomposite polymer films," *Polymer Journal*, vol. 42, no. 12, pp. 935–940, 2010.

[19] Y. Nakanishi, A. Miyake, H. Kominami, T. Aoki, Y. Hatanaka, and G. Shimaoka, "Preparation of ZnO thin films for high-resolution field emission display by electron beam evaporation," *Applied Surface Science*, vol. 142, no. 1, pp. 233–236, 1999.

[20] G.-H. Ning, X.-P. Zhao, J. Li, and C.-Q. Zhang, "Hugely enhanced electroluminescence from mesoporous ZnO particles," *Optical Materials*, vol. 28, no. 4, pp. 385–390, 2006.

[21] S. Saha, S. K. Arya, S. P. Singh, and V. Gupta, "A novel ZnO-methylene blue nanocomposite matrix for biosensing application," *International Journal of Electrochemistry*, vol. 2011, Article ID 823734, 6 pages, 2011.

[22] G. Gustafsson, Y. Cao, G. M. Treacy, F. Klavetter, N. Colaneri, and A. J. Heeger, "Flexible light-emitting diodes made from soluble conducting polymers," *Nature*, vol. 357, no. 6378, pp. 477–479, 1992.

[23] Z.-X. Xu, V. A. L. Roy, P. Stallinga et al., "Nanocomposite field effect transistors based on zinc oxide/polymer blends," *Applied Physics Letters*, vol. 90, no. 22, Article ID 223509, 2007.

[24] A. Di Mauro, M. Zimbone, M. Scuderi, G. Nicotra, M. E. Fragalà, and G. Impellizzeri, "Effect of Pt nanoparticles on the photocatalytic activity of ZnO nanofibers," *Nanoscale Research Letters*, vol. 10, article 484, 2015.

[25] L. Zhang, H. Sun, L. Xie et al., "Inorganic solar cells based on electrospun ZnO nanofibrous networks and electrodeposited Cu_2O," *Nanoscale Research Letters*, vol. 10, article 465, 2015.

[26] J. Wang, X. Wei, and P. Wangyang, "Gas-sensing devices based on Zn-doped NiO two-dimensional grainy films with fast response and recovery for ammonia molecule detection," *Nanoscale Research Letters*, vol. 10, no. 1, article 461, pp. 1–9, 2015.

[27] I. I. P. C. Buzea and K. Robbie, "Nanomaterials and nanoparticles: sources and toxicity," *Biointerphases*, vol. 2, pp. 17–71, 2007.

[28] A. Sirelkhatim, S. Mahmud, A. Seeni et al., "Review on zinc oxide nanoparticles: antibacterial activity and toxicity mechanism," *Nano-Micro Letters*, vol. 7, no. 3, pp. 219–242, 2015.

[29] R. Brayner, R. Ferrari-Iliou, N. Brivois, S. Djediat, M. F. Benedetti, and F. Fiévet, "Toxicological impact studies based on *Escherichia coli* bacteria in ultrafine ZnO nanoparticles colloidal medium," *Nano Letters*, vol. 6, no. 4, pp. 866–870, 2006.

[30] J. T. Seil and T. J. Webster, "Antimicrobial applications of nanotechnology: methods and literature," *International Journal of Nanomedicine*, vol. 7, pp. 2767–2781, 2012.

[31] S. Reddy, N. Bananakere, and H. J. Chandrashekar, "Cationic surfactants-assisted synthesis of ZnO nanoparticles and their modified carbon paste electrode for electrochemical investigation of dopamine," *Analytical and Bioanalytical Electrochemistry*, vol. 4, pp. 186–196, 2012.

[32] V. R. Gaevs'ky, N. Yu, K. Y. Novoselets, and B. P. Rudyk, "Electrolytic fabrication of zinc oxide nanoparticles," *Ukrainian Journal of Physics*, vol. 58, no. 4, pp. 385–388, 2013.

[33] A. Gupta, P. Srivastava, L. Bahadur, D. P. Amalnerkar, and R. Chauhan, "Comparison of physical and electrochemical properties of ZnO prepared via different surfactant-assisted precipitation routes," *Applied Nanoscience*, vol. 5, no. 7, pp. 787–794, 2015.

[34] Y.-J. Hsiao, T.-H. Fang, L.-W. Ji, and B.-Y. Yang, "Red-shift effect and sensitive responsivity of MoS_2/ZnO flexible photodetectors," *Nanoscale Research Letters*, vol. 10, article 443, 2015.

[35] W.-D. Hsu, J.-K. Tsai, T.-H. Meen, T.-C. Wu, Y.-K. He, and Y.-D. Lai, "Self-etching-induced morphological evolution of ZnO microrods grown on FTO glass by hydrothermal method," *Nanoscale Research Letters*, vol. 10, no. 1, article 428, 2015.

[36] A. A. Negahdary, S. Mehrtashfar, M. Imandar, H. Akbari-Dastjerdi, A. Jamaleddini, and M. Ajdary, "A biosensor for determination of H_2O_2 by use of HRP enzyme and modified CPE with ZnO NPs," *International Journal of Electrochemical Science*, vol. 7, pp. 5185–5194, 2012.

[37] X. Fuku, B. Singh, R. F. Ajayi et al., "A gallium telluride quantum dots bioelectrode system for human epidermal growth factor receptor-2 (Her2/neu) oncogene signalling," *Analytical Methods*, vol. 7, no. 15, pp. 6114–6124, 2015.

[38] A. K. Singh, "Synthesis, characterization, electrical and sensing properties of ZnO nanoparticles," *Advanced Powder Technology*, vol. 21, no. 6, pp. 609–613, 2010.

[39] D. Sridevi and K. V. Rajendran, "Synthesis and optical characteristics of ZnO nanocrystals," *Bulletin of Materials Science*, vol. 32, no. 2, pp. 165–168, 2009.

[40] S. Talam, S. R. Karumuri, and N. Gunnam, "Synthesis, characterization, and spectroscopic properties of ZnO nanoparticles," *ISRN Nanotechnology*, vol. 2012, Article ID 372505, 6 pages, 2012.

[41] W.-Y. Wu, J.-M. Ting, and P.-J. Huang, "Electrospun ZnO nanowires as gas sensors for ethanol detection," *Nanoscale Research Letters*, vol. 4, no. 6, pp. 513–517, 2009.

[42] S. O. Fatin, H. N. Lim, W. T. Tan, and N. M. Huang, "Comparison of photocatalytic activity and cyclic voltammetry of zinc oxide and titanium dioxide nanoparticles toward degradation of methylene blue," *International Journal of Electrochemical Science*, vol. 7, no. 10, pp. 9074–9084, 2012.

[43] M. Starowicz and B. Stypuła, "Electrochemical synthesis of ZnO nanoparticles," *European Journal of Inorganic Chemistry*, vol. 5, no. 6, pp. 869–872, 2008.

[44] G. R. Navale, D. J. Late, and S. S. Shinde, "Antimicrobial activity of ZnO nanoparticles against pathogenic bacteria and fungi," *Nanotechnology Nanomedical*, vol. 3, article 1033, 2015.

[45] Y. Liu, L. He, A. Mustapha, H. Li, Z. Q. Hu, and M. Lin, "Antibacterial activities of zinc oxide nanoparticles against *Escherichia coli* O157:H7," *Journal of Applied Microbiology*, vol. 107, no. 4, pp. 1193–1201, 2009.